Geometry-induced fractal behaviour in a semiconductor billiard

1998 J. Phys.: Condens. Matter 10 1339

(http://iopscience.iop.org/0953-8984/10/6/016)

J. Phys.: Condens. Matter **10** (1998) 1339–1347. Printed in the UK PII: S0953-8984(98)86240-1

Geometry-induced fractal behaviour in a semiconductor billiard

A P Micolich†¶, R P Taylor†, R Newbury†, J P Bird‡, R Wirtz†, C P Dettmann§, Y Aoyagi‖ and T Sugano‖

† School of Physics, University of New South Wales, Sydney 2052, Australia
‡ Center for Solid State Research, Arizona State University, Tempe, AZ 85287-6206, USA
§ Department of Physics and Astronomy, Northwestern University, Evanston, IL 60208, USA
‖ Nanoelectronics Materials Laboratory, RIKEN, 2-1 Hirosawa, Wako-shi, Saitama 351-01, Japan

Received 22 July 1997, in final form 23 October 1997

Abstract. We report geometry-induced fractal behaviour in the low-field magneto-conductance fluctuations of a mesoscopic semiconductor billiard. Such fractal behaviour was recently predicted to be induced by the mixed (chaotic/regular) phase space generated by the soft-walled billiard potential, and our results constitute a possible experimental observation of the infinite hierarchical nature of this mixed phase space. Preliminary investigations of the effects of temperature and gate bias, which directly control the electron coherence and billiard potential profile, are presented.

Due to the long electron mean free paths found in AlGaAs/GaAs heterostructures, mesoscopic billiards provide an ideal environment for studies of electron quantum interference (QI) phenomena [1]. Application of a negative bias to metal gates deposited on the heterostructure surface leads to electron depletion in regions directly below the gates. Hence sub-micron cavities (billiards) can be defined in the two-dimensional electron gas (2DEG) at the AlGaAs/GaAs interface. Electrons injected into these billiards travel ballistically, with trajectories predominantly determined by the billiard geometry rather than material-related scattering processes [2, 3]. At low temperatures, electrons preserve their phase coherence whilst traversing the billiard, and semiclassical QI effects, such as magneto-conductance fluctuations (MCF), result from pairs of trajectories which form closed loops [4]. A recent semiclassical theory suggests that MCF observed in mesoscopic electron systems are fractal [5] due to the trajectory trapping effect of regions of mixed (chaotic/integrable) phase space. Fractal MCF have been observed in the quasi-ballistic scattering regime in gold nano-wires [6]. In this paper, we report the observation of geometry-induced fractal MCF in the fully ballistic scattering regime of a mesoscopic semiconductor billiard. We discuss this new phenomenon in terms of the physical factors which determine the fractal dimension D_F of the system [7]. Fractal analysis of MCF is performed using four techniques to obtain an accurate estimate of the D_F-dependence on experimental parameters such as the temperature, which limits the phase coherence in QI processes, and gate bias V_G, which determines the potential profile of the billiard. There

¶ Fax: +61-2-9385-6060; e-mail: mico@lenz.phys.unsw.edu.au.

0953-8984/98/061339+09$19.50

has been considerable theoretical interest in the prediction of D_F for a given system. The D_F-values obtained from this device agree with those predicted for billiards defined by a soft-wall potential profile [5].

For billiards approximated by a hard-wall description (a flat-bottomed billiard shaped by walls of infinite height), the cavity geometry determines whether the electron classical trajectories are chaotic or regular [2, 3, 8, 9]. Electron dynamics in a square billiard are nominally regular with an escape probability distribution governed by a power law $P(t) \propto t^{-\gamma}$ where $\gamma > 2$. Since the area contained by closed trajectory loops is dependent on the time preceding electron escape from the billiard, regular billiards support a similar area distribution, $P(A) \propto A^{-\beta}$ with $\beta > 2$ [10]. In a semiclassical picture, $P(A)$ determines the magnetic field period (ΔB) content of the MCF structure through $\Delta B = h/eA$ [4, 11]. Recent theoretical investigations [5] have shown that soft-walled confining potentials, which define semiconductor billiards, produce a mixed (chaotic/regular) phase space. The escape of electron trajectories is then blocked by the infinite hierarchy of Cantori which occur at the chaotic/regular boundary, resulting in $P(A) \propto A^{-\beta}$ with $\beta \leqslant 2$. For $\beta \leqslant 2$, the statistical properties of the magneto-conductance match those of a Gaussian random process with variance of the increments ΔB given by $\langle(\Delta G)^2\rangle \propto (\Delta B)^{\beta}$ and $\langle \Delta G\rangle = 0$. In these expressions, $\Delta G = \delta G(B) - \delta G(B + \Delta B)$ with $\delta G = G(B) - \langle G(B)\rangle$ [5, 7]. The averaging $\langle\ \rangle$ is performed over B. Such processes are termed fractional Brownian motion and produce a fractal trace with dimension

$$D_F = 2 - \frac{\beta}{2} \tag{1}$$

where $1 < D_F < 2$ [5, 7]. In contrast, for $\beta > 2$ the variance follows the relation $\langle(\Delta G)^2\rangle \sim (\Delta B)^2$ and fractal behaviour is not predicted. The observation of fractal MCF is restricted to a finite-B field range. Semiclassical theories assume that on the scale of the fluctuations the magnetic field induces changes only in the phases of the electron waves (due to the introduction of the magnetic vector potential) and not in the curvature of the classical trajectories [4]. At the magnetic field B_{cyc}, the curvature of the trajectories is sufficient that the classical cyclotron orbit can fit within the square. MCF at fields higher than this arise from trajectories which form skipping orbits [12] and in this paper we concentrate on fields below B_{cyc}. Within this field range, the fractal behaviour is predicted to be limited to field scales $\Delta B < B_C$. The correlation field B_C is determined from $F(B_C) = F(0)/2$ where $F(\Delta B) = \langle \delta G(B)\, \delta G(B + \Delta B)\rangle$ is the autocorrelation function [5, 6, 12]. $F(\Delta B)$ is related to the variance by the expression $F(\Delta B) = F(0) - (1/2)\langle(\Delta G)^2\rangle$ [6]. This limits the largest field scale over which fractal behaviour is observed, and later we discuss the factors which limit the smallest scale. We note that the above fractal behaviour implies statistical self-similarity in the MCF. A subset of statistical self-similarity is the exact self-similarity recently observed in the magneto-conductance of a semiconductor Sinai billiard [13, 14]. The properties and physical conditions necessary for exact self-similarity have been presented elsewhere [14].

To observe the predicted fractal behaviour, we consider the gate geometry shown in figure 1, inset (a), which defines a 1 μm square billiard in the 2DEG located 71 nm below the heterostructure surface. Quantum point contacts (QPCs) with lithographic width 0.1 μm serve as entrance and exit ports. The billiard is significantly shorter than the electron mean free path of $\sim$3 μm and electrons travel ballistically through the device. Experiments were performed at lattice temperatures T in the range 30 mK–4 K. Measurements of device electrical resistance as a function of magnetic field applied perpendicular to the 2DEG were made using a low-frequency four-terminal a.c. measuring technique. The magneto-conductance appears as reproducible fluctuations superimposed on a slowly varying

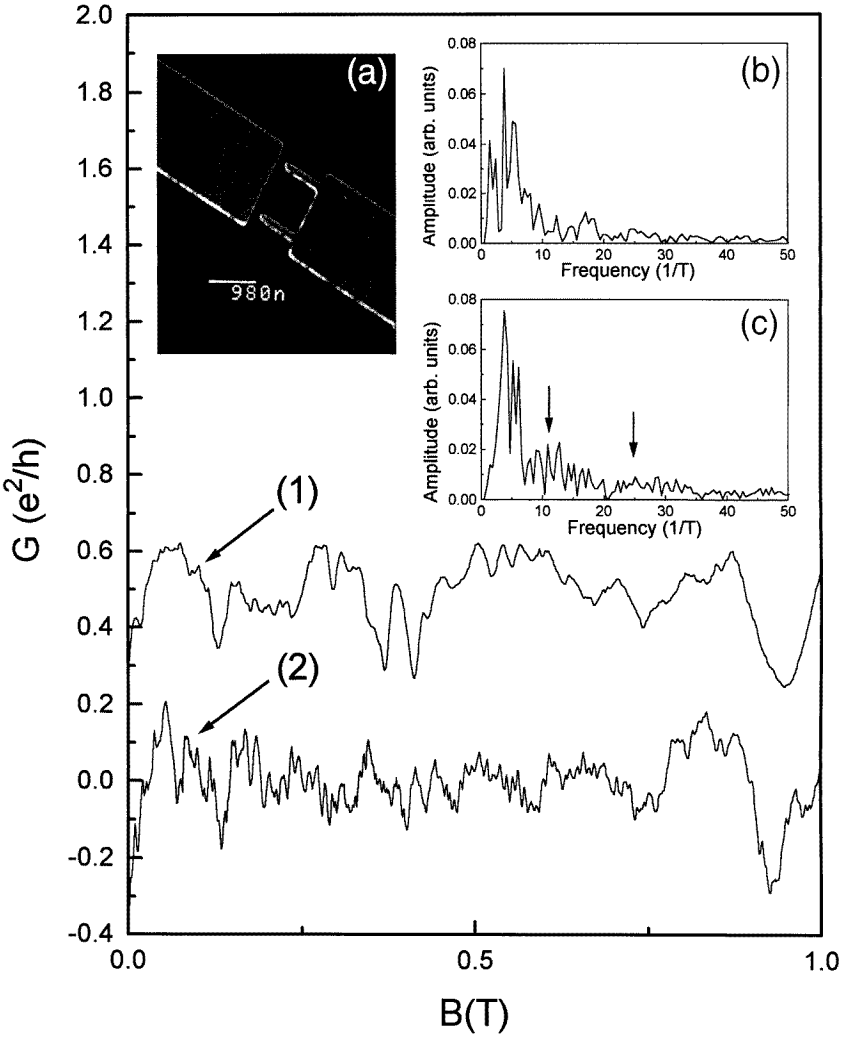

Figure 1. MCF obtained from a 1 μm billiard with (1) $T = 3.8$ K and (2) $T = 30$ mK. Insets: (a) a scanning electron micrograph of our billiard; the spacer bar indicates $\sim$1 μm; (b), (c) Fourier transforms of MCF (1) and (2) respectively. Arrows indicate regions with increased high-frequency MCF component at $T = 30$ mK.

background signal. This background is removed by a polynomial fit subtraction and converted to conductance prior to analysis, a standard technique for studies of MCF [12]. The resulting MCF trace has the property $\langle G(B) \rangle = 0$. Figure 1 displays typical data at temperatures of (1) $T = 3.8$ K and (2) $T = 30$ mK. Rich structure appears in the 30 mK trace: this broad spectrum of frequency components produces structure on finer and finer field scales, and therefore raises the question of whether the MCF pattern has a fractal quality. The respective Fourier transforms (figure 1, insets (b), (c)) demonstrate the damping of higher-frequency components of the MCF with increasing temperature, and hence we would expect D_F to be temperature dependent. The analysis below, which quantifies this prediction, is restricted to the parameter ranges $B < B_{cyc} = 0.2$ T and

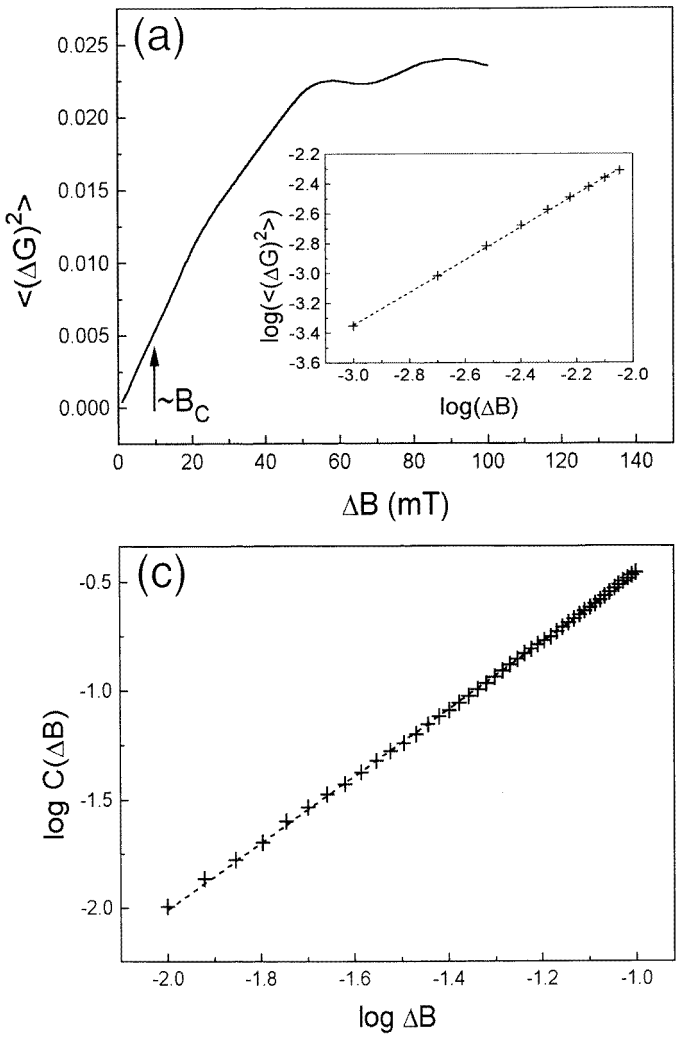

Figure 2. (a) $\langle(\Delta G)^2\rangle$ versus ΔB averaged over $B = 0$–0.2 T. The region $\Delta B < B_C$ is used to determine D_F^{var}. Inset: $\log(\langle(\Delta G)^2\rangle)$ versus $\log \Delta B$ used to obtain β. (b) $-\log N(\Delta B)$ versus $\log \Delta B$ used to obtain D_F^{box}. (c) $\log C(\Delta B)$ versus $\log \Delta B$ used to obtain D_F^{cor}. (d) A plot of $L(\Delta B)$ versus ΔB showing a lack of convergence to a fixed length with decreasing ΔB for the MCF, indicative of fractal behaviour. Inset: $\log L(\Delta B)$ versus $\log \Delta B$ obtained after analysing the MCF and a straight line as marked. D_F^{coast} is obtained from the line of best fit (dashed).

$\Delta B < B_C \sim 10$ mT, as required by the semiclassical theory.

Fractal analysis is performed using four (variance, box counting, correlation and coastline) techniques to establish consistent behaviour of D_F as experimental parameters are adjusted. In general, fractal patterns are generated on the basis of a power-law relationship [7, 15] between the statistics of the MCF being assessed (see below) and the increment in magnetic field ΔB, and the fractal dimension is extracted from the power-law exponent. This quality of fractal MCF is true both for the statistical self-similarity discussed here and the exact self-similarity presented elsewhere [13, 14]. The variance technique used to calculate the 'variance' fractal dimension D_F^{var} is based directly on the

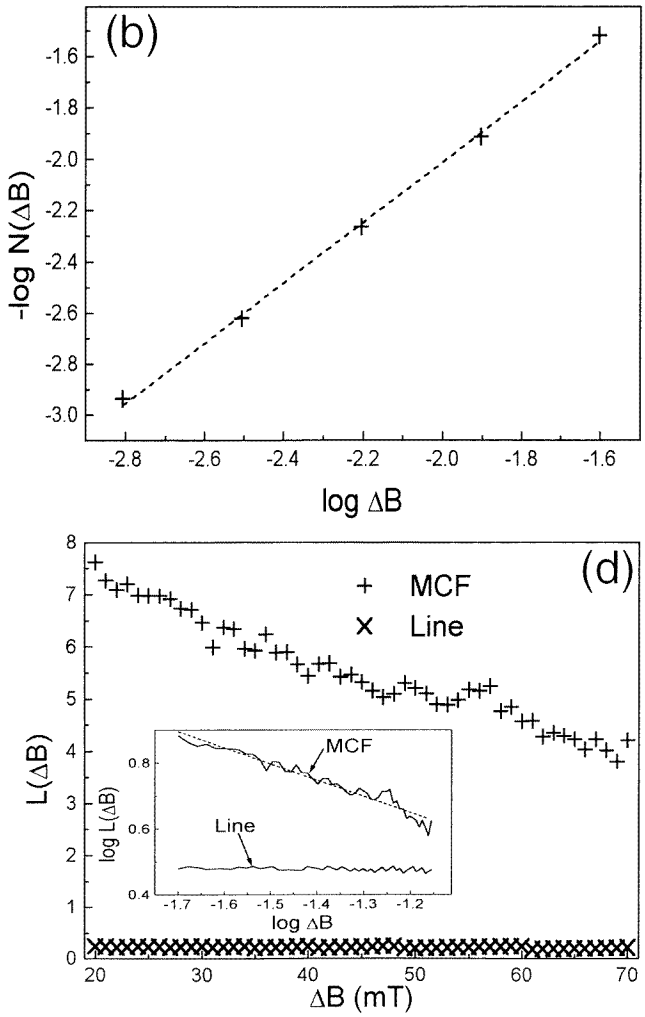

Figure 2. (Continued)

theoretical investigations presented above. In figure 2(a) we plot $\langle(\Delta G)^2\rangle$ versus ΔB over the range $\Delta B_R < \Delta B < 100$ mT. ΔB_R is the magnetic field resolution of 1 mT. In the limit $\Delta B < B_C$, β can be extracted from a linear fit of the plot $\log(\langle(\Delta G)^2\rangle)$ versus $\log(\Delta B)$, as shown in figure 2(a), inset. The fractal dimension D_F^{var} is then obtained via equation (1).

The 'capacity' fractal dimension D_F^{box} is evaluated using a box-counting technique, where a mesh of boxes (or 'cells') is placed over the MCF as follows. The magnetic field range of the MCF data is divided into n segments each of width ΔB. The conductance range of the data (determined from the maximum and minimum values of δG) is then divided into n segments, creating a mesh of $n \times n$ boxes. A count of the number of boxes $N(\Delta B)$ containing part of the data trace is made as the mesh becomes increasingly finer until ΔB reaches the magnetic field resolution ΔB_R. D_F^{box} is defined by the power law

$$N(\Delta B) = \lim_{\Delta B \to 0} k(\Delta B)^{-D_F^{box}}$$

where k is a proportionality constant [15]. The fractal dimension for this technique is then given by

$$D_{\mathrm{F}}^{\mathrm{box}} = \lim_{\Delta B \to 0} \frac{\log N(\Delta B)}{\log(\Delta B)}. \tag{2}$$

Hence $D_{\mathrm{F}}^{\mathrm{box}}$ is obtained by a linear fit to $-\log N(\Delta B)$ versus $\log \Delta B$ in the low-ΔB limit, as shown in figure 2(b).

The 'correlation' dimension $D_{\mathrm{F}}^{\mathrm{cor}}$ is calculated using a method similar to the box-counting technique. A circle of radius ΔB is defined around each discrete point i in the data set and the number $P_{ij}(\Delta B)$ of other data points j lying within it is counted. The correlation function $C(\Delta B)$ is then the sum of $P_{ij}(\Delta B)$ over the set of data points j such that

$$C(\Delta B) = \frac{1}{N^2} \sum_{i,j=1}^{N} P_{ij}(\Delta B) \tag{3}$$

and N is the total number of data points. We note that $C(\Delta B)$ is defined such that $C(\Delta B) = 1$ if all of the data points lie within ΔB of each other. If ΔB is less than the smallest interval between data points, then $P_{ij}(\Delta B) = 0$ and $C(\Delta B) = 0$ [15]. A trivial case of the latter is for $\Delta B < \Delta B_{\mathrm{R}}$ and hence this method is restricted to increments $\Delta B > \Delta B_{\mathrm{R}}$ [15]. The correlation dimension is defined by the power law

$$C(\Delta B) = \lim_{\Delta B \to 0} k(\Delta B)^{-D_{\mathrm{F}}^{\mathrm{cor}}}$$

where k is a proportionality constant [15]. Hence

$$D_{\mathrm{F}}^{\mathrm{cor}} = \lim_{\Delta B \to 0} \frac{\log C(\Delta B)}{\log(\Delta B)}. \tag{4}$$

$D_{\mathrm{F}}^{\mathrm{cor}}$ is obtained by a linear fit of $\log C(\Delta B)$ versus $\log \Delta B$ in the limit $\Delta B \to 0$, as shown in figure 2(c).

The 'coastline' dimension follows that used by Richardson and later Mandelbrot in their original work on coastlines [7], where a pair of dividers set to a length ε is used to determine the coastline length $L(\varepsilon)$. The length $L(\varepsilon)$ is given by $q \times \varepsilon$, where q is the number of steps along the coastline made by the dividers. We use a similar approach computationally to obtain $L(\Delta B)$ for $\Delta B > \Delta B_{\mathrm{R}}$. As displayed in figure 2(d), the length $L(\Delta B)$ steadily increases for the MCF trace as ΔB is reduced, which is typical of fractal behaviour. The coastline dimension is obtained from the power-law relationship

$$L(\Delta B) = \lim_{\Delta B \to 0} k(\Delta B)^{1-D_{\mathrm{F}}^{\mathrm{coast}}}$$

where again k is a constant of proportionality [7]. Hence

$$D_{\mathrm{F}}^{\mathrm{coast}} = 1 - m \tag{5}$$

where m is the slope of $\log L(\Delta B)$ versus $\log \Delta B$ in the limit $\Delta B \to 0$. Plots of $\log L(\Delta B)$ versus $\log \Delta B$ are shown in figure 2(d), inset, for a typical data set (sloped line). We also show for comparison the same analysis performed on a straight line (non-fractal) where the length $L(\Delta B)$ converges to a fixed value and with a gradient $m = 0$, as expected. The jagged nature of these graphs is due to the length-measuring process being restricted to integer multiples of the length increment ΔB. This artefact of the analysis leads to some uncertainty in the linear fits for smaller data sets and causes scatter in the $D_{\mathrm{F}}^{\mathrm{coast}}$-values presented.

The results of fractal analysis of the MCF obtained at different T and V_{G} are displayed in table 1. The pair of values listed for each experimental condition are obtained by sweeping

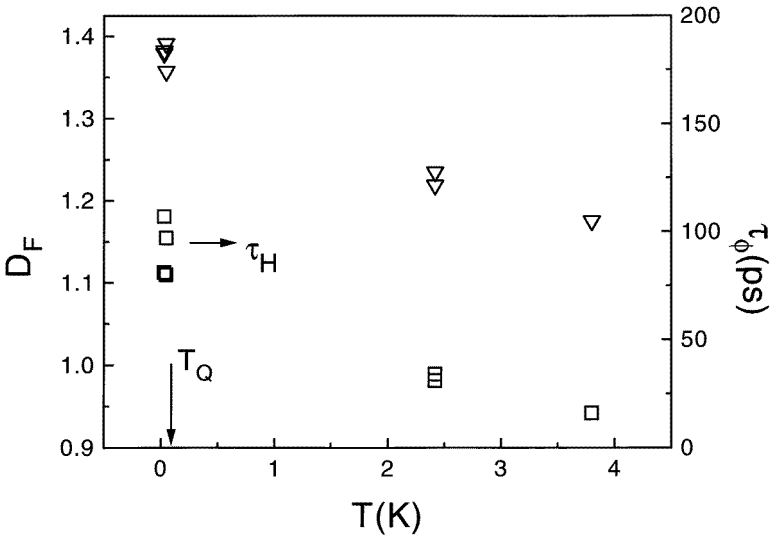

Figure 3. A plot of the average effective D_F (left-hand axis, $\triangledown$) and τ_ϕ (right-hand axis, $\square$) versus T. $T_Q \sim 105$ mK and $\tau_H \sim 95$ ps are marked.

Table 1. D_F for each analysis technique, average D_F, τ_ϕ and l_ϕ for various T and V_G.

T (K)	V_G (V)	D_F^{var}	D_F^{box}	D_F^{cor}	D_F^{coast}	Average D_F	τ_ϕ (ps)	l_ϕ (μm)
2.42	−0.64	1.31	1.03	1.20	1.33	1.22	31	8.5
2.42	−0.64	1.31	1.05	1.23	1.36	1.24	34	9.3
0.05	−0.64	1.44	1.17	1.52	1.30	1.36	97	26.6
0.05	−0.64	1.45	1.18	1.54	1.40	1.39	80	22.0
0.03	−0.6	1.47	1.23	1.51	1.31	1.38	81	22.2
0.03	−0.6	1.49	1.19	1.49	1.35	1.38	107	29.4
3.8	−0.6	1.34	1.01	1.11	1.24	1.18	16	4.4

the magnetic field in opposite directions. Due to the Onsager relations [1], the MCF are symmetric about $B = 0$ T and therefore a comparison of the D_F-values within each pair is indicative of the noise level. This is typically less than 2–3% [16]. For all of the parameters $1 < D_F < 2$, as required for fractal behaviour. It is important to consider the physical limitations which may lead to an 'effective' value lower than the true fractal dimension induced by the billiard geometry. Theoretical expressions for each of the analysis techniques specify that the linear fit be taken in the limit where the field increment ΔB approaches zero. This requirement implies infinite data resolution. In experiments, data consist of a finite number of data points between which some form of interpolation is used. Below ΔB_R, fractal analysis detects the interpolation which is inherently non-fractal. This leads to an effective D_F-value lower than the true fractal dimension of the data. Aside from experimental limitations, there are other physical factors affecting assessments of fractal behaviour at a finite temperature T. The phase coherence length l_ϕ establishes an upper limit on the accumulated trajectory area, limiting the smallest ΔB of the MCF [4]. Analysis of the phase-breaking time [12] gives $\tau_\phi \sim 90$ ps at 30 mK, corresponding to $l_\phi = v_F \tau_\phi \sim 24$ μm. As an estimate, if we consider a typical diamond-shaped periodic orbit of length 2.8 μm for our billiard [17], we expect ∼8 orbits before phase coherence

is lost and the electron no longer contributes to QI processes. This provides an upper area limit of 4 μm^2 and a corresponding smallest MCF period component of $\Delta B_{\rm min} \sim 1$ mT. Therefore at 30 mK, $\Delta B_{\rm min} \sim \Delta B_{\rm R}$. With increasing T, thermally induced scattering processes decrease τ_ϕ (as seen in figure 3) resulting in smaller maximum loop areas and an increase in $\Delta B_{\rm min}$, as evident from figure 1. Damping of MCF structure leads to a decrease in the effective $D_{\rm F}$ provided that $\Delta B_{\rm min} > \Delta B_{\rm R}$. This condition is satisfied for $T > 30$ mK and figure 3 confirms the expected reduction in $D_{\rm F}$ with T. We note that τ_ϕ and $D_{\rm F}$ follow a strikingly similar evolution with T. Naively, assuming infinite field resolution, this trend suggests that extrapolation towards $T = 0$ would result in an infinite spectrum of MCF frequencies and the observation of purely geometry-induced (i.e. $P(A) \propto A^{-\beta}$) fractal behaviour. However, the semiclassical approximation is predicted to break down for temperatures below $T_{\rm Q} = \Delta E/k_{\rm B} = 2\pi\hbar^2/m^* k_{\rm B} A_{\rm B} \sim 105$ mK ($A_{\rm B}$ is the area of the billiard and ΔE the energy level spacing), where the discrete energy level structure of the billiard becomes resolved [18], and deviations from semiclassical theory are expected. For $T < T_{\rm Q}$ a saturation of τ_ϕ has been observed [18, 19], with a saturation value which approximates to the Heisenberg time $\tau_{\rm H} = \hbar/k_{\rm B}T_{\rm Q}$ [18]. Although further data are required to establish a saturation trend, we note that below $T_{\rm Q}$, τ_ϕ agrees with $\tau_{\rm H} \sim 95$ ps for our billiard. Saturation of τ_ϕ for $T < T_{\rm Q}$ means that the frequency spectrum of the MCF will remain constant, and an associated saturation in the effective $D_{\rm F}$-value is expected. Further experiments are planned to investigate the possibility of $D_{\rm F}$-saturation beyond the semiclassical limit.

The electrostatic definition of the billiard implies that adjustments in $V_{\rm G}$ change the billiard potential profile and the mixed phase space responsible for the observed fractal behaviour [5]. Hence we expect $V_{\rm G}$ to be effective in tuning the observed geometry-induced fractal behaviour. As $V_{\rm G}$ is adjusted from -0.64 V to -0.6 V, a change in the weak-localization peak lineshape [9] is observed, indicating a geometry-induced change in the electron dynamics. An associated change in $D_{\rm F}$-values is also observed, as shown in table 1. This is not related to the $\sim$20 mK difference between the data sets, as τ_ϕ has saturated at this temperature. Rather, we suggest that adjustments in the potential profile associated with changing $V_{\rm G}$ alter the phase space and the trajectory trapping effect responsible for the fractal behaviour. Experiments are planned to investigate the effect of $V_{\rm G}$ more closely, and theoretical simulations accounting for soft-walled potentials are in progress.

In conclusion, we report the observation of geometry-induced fractal behaviour in the magneto-conductance of a mesoscopic semiconductor billiard. This fractal behaviour is consistent with recent semiclassical theory investigating the trapping of trajectories by the infinite hierarchy of Cantori formed at the chaotic/regular boundary of the mixed phase space generated by soft-walled confining potentials in the billiard. Observations of the temperature behaviour indicate an increasing effective $D_{\rm F}$ with decreasing temperature for $T > T_{\rm Q}$, where the discrete energy levels become resolved. This temperature dependence is associated with increasing phase coherence length raising the MCF frequency content. We also note a change in $D_{\rm F}$ with $V_{\rm G}$, demonstrating the association between fractal behaviour and billiard potential profile.

Acknowledgment

We thank G P Morriss for valuable discussions.

References

[1] Beenakker C W J and Van Houten H 1991 Quantum transport in semiconductor nanostructures *Solid State Physics* vol 44 (New York: Academic) p 1

[2] Marcus C M, Rimberg A J, Westervelt R M, Hopkins P F and Gossard A C 1992 *Phys. Rev. Lett.* **69** 506

[3] Chang A M, Baranger H U, Pfeiffer L N and West K N 1994 *Phys. Rev. Lett.* **73** 2111

[4] Jalabert R A, Baranger H U and Stone A D 1990 *Phys. Rev. Lett.* **65** 2442

[5] Ketzmerick R 1996 *Phys. Rev.* B **54** 10 841

[6] Hegger H, Hecker K, Reckziegel G, Freimuth A, Huckestein B, Janssen M and Tuzinski R 1996 *Phys. Rev. Lett.* **77** 3885

[7] Mandelbrot B 1982 *The Fractal Geometry of Nature* (San Francisco, CA: Freeman)

[8] Baranger H U, Jalabert R A and Stone A D 1990 *Phys. Rev. Lett.* **70** 3876

[9] Bird J P, Olatona D M, Newbury R, Taylor R P, Ishibashi K, Stopa M, Aoyagi Y, Sugano T and Ochiai Y 1995 *Phys. Rev.* B **52** R14 336

[10] Jensen R V 1991 *Chaos* **1** 101

[11] Aharonov Y and Bohm D 1959 *Phys. Rev.* **115** 485

[12] Bird J P, Ishibashi K, Ferry D K, Newbury R, Olatona D M, Ochiai Y, Aoyagi Y and Sugano T 1996 *Surf. Sci.* **361/362** 730

[13] Taylor R P, Newbury R, Sachrajda A S, Feng Y, Coleridge P T, Dettmann C, Zhu Ningjia, Guo Hong, Delage A, Kelly P J and Wasilewski Z 1997 *Phys. Rev. Lett.* **78** 1952

[14] Taylor R P, Micolich A P, Newbury R and Fromhold T M 1997 *Phys. Rev.* B **56** 1

[15] Hilborn R C 1994 *Chaos and Nonlinear Dynamics* (Oxford: Oxford University Press)

[16] Note: within each pair, the two sets of data were also taken more than 12 hours apart, demonstrating the stability of the device and measuring process.
Taylor R P 1994 *Nanotechnology* **5** 183

[17] Akis R, Bird J P and Ferry D K 1996 *J. Phys.: Condens. Matter* **8** L667

[18] Clarke R M, Chan I H, Marcus C M, Duruoz C I, Harris J S Jr, Campman K and Gossard A C 1995 *Phys. Rev.* B **52** 2656

[19] Bird J P, Linke H, Cooper J, Micolich A P, Ferry D K, Akis R, Ochiai Y, Taylor R P, Newbury R, Omling P, Aoyagi Y and Sugano T 1997 *Phys. Status Solidi* b **204** 314